catalysts

MDPI

Article

Application of Supported TiO_2 in Carbonated Binding Material and Its Photocatalytic Performance

Heyang Si [1,2], Yongle Fang [2] and Lu Yang [1,*]

[1] State Key Laboratory of Silicate Materials for Architectures, Wuhan University of Technology, 122# Luoshi Road, Wuhan 430070, China; siheyang@whut.edu.cn

[2] School of Materials Science and Engineering, Wuhan University of Technology, Wuhan 430070, China; 290585@whut.edu.cn

* Correspondence: yanglu@whut.edu.cn

Received: 17 October 2020; Accepted: 14 November 2020; Published: 17 November 2020

Abstract: Although photocatalytic concrete can significantly contribute to the degradation of air pollutants and improving the sustainability levels, the complexity of ordinary cement system often caused the uncertain performance of mixed photocatalysts, which limited the real application of photocatalysts. Since the rapid carbonization hardening and relatively simple composition, γ-C_2S carbonated binding material has gained considerable attention for its application in construction material. In this work, quartz sand-supported TiO_2-C_2S(γ) composites (TQSC) were prepared by mixing photocatalytic quartz sand with γ-C_2S and mounting in γ-C_2S matrix surface methods. The TiO_2-coated quartz sand (TQS) was characterized by X-ray diffraction (XRD), quantitative X-ray fluorescence (XRF) and scanning electron microscopy (SEM). The photocatalytic performance and durability (washing resistance) of TQSC were also investigated by the degradation ability of NOx and rhodamine B (RhB). The results show that a uniform TiO_2 layer on quartz sand was prepared, and the photocatalytic De-NOx (degradation of NOx) performance increased with increasing the mounted amounts of TiO_2/quartz sand in γ-C_2S carbonated matrix surface, but would decrease the photocatalytic durability. After water-washing, the De-NOx efficiencies of TQSC specimens decreased quickly at the beginning, which were adhering to the mounted amounts of TiO_2/quartz sand, but would become stable after water-washing for 3600 s for all samples. The relatively high De-NOx stability and good self-cleaning effect of the water-washed TQSC-60% specimen can be considered a promising photocatalytic product for real applications.

Keywords: photocatalytic concrete; γ-C_2S carbonated binding material; supported TiO_2; NOx; photocatalytic durability

1. Introduction

Acid rain and photochemical smog have been identified the most critical environmental problems in modern society, which usually caused by the gaseous pollutants such as NOx, SOx [1–3], etc. Of which, as one of the most common gaseous pollutants, NOx—mainly NO and NO_2—primarily emitted from industrial and traffic, are the major source of photochemical smog. This produces a negative impact on our ecosystem and human health, as well as affecting buildings and industries [4–6]. Consequently, finding ways to abate the NOx atmospheric pollutants on a large scale is essential, and has attracted more and more attention in recent years.

As a promising technology to purify NOx harmful pollutants, photocatalytic oxidation (PCO) has been considered in the past [7,8]. Among available photocatalysts, titanium dioxide (TiO_2) is the most commonly investigated due to its excellent chemical stability, high oxidizing ability and relatively low price [9–13]. The introduction of TiO_2 into building materials is one of the directions for NOx degradation

by using the adequate large exposed area of construction [14,15]. The incorporation methods of TiO_2 as a photocatalyst in construction, mainly in cementitious material, can be divided into three categories: (i) blended TiO_2 photocatalyst with cement, and then applied to the surface of mortar layer, (ii) sprayed TiO_2 suspension on the surface of hardened mortar, and (iii) directly coated TiO_2 photocatalytic powder on the surface of fresh mortar [16–19]. It has been demonstrated that a photocatalyst coating on the surface of cementitious materials is an effective way to promote photocatalytic efficiency [20–22]. However, the photocatalytic coatings susceptibly suffer from environmental abrasion, which limit their long-term application effects [23]. On the other hand, many useful studies also indicate that the efficiency of a photocatalyst can be adversely affected by the properties of Portland cementitious materials due to the low specific surface areas of cement, carbonization of surface, agglomeration of photocatalyst particles, diversified ion species and pH value in cement-based systems [24–32]. Through regulating the matrix microstructure, surface and TiO_2 photocatalyst modifications, the photocatalytic ability of the photocatalytic cementitious materials can be efficiently increased [33–36], while the inherent cement environmental effects and relatively high cost of TiO_2 photocatalysts are still the main limitations to the widespread application of photocatalytic cementitious materials.

Recently, the applications of gamma polymorph of dicalcium silicate (γ-C_2S) in building materials have gained significant attention [37]. γ-C_2S has inert hydration activity but high carbonation reactivity [38]; the carbonization products of γ-C_2S contain calcium carbonates (calcite and aragonite) and amorphous silica gels in the presence of moisture and CO_2 [39,40], indicates the excellent environment friendly of this material. Because of the carbonation, γ-C_2S carbonated matrix surface has a relative stable chemical environment, and $CaCO_3$ mainly provides the chance for the long-term application of TiO_2 photocatalysts, which avoids the adverse effects of cement hydrates. Our previous work [41] also reveals that the hygroscopicity of $CaCO_3$ and silica gel can change the moisture of photocatalytic materials, which are beneficial to the improvement De-NOx selectivity.

The complexity of ordinary Portland cement system often caused the uncertain performance of mixed photocatalysts, which limited the real application of photocatalysts, while the rapid carbonization hardening and relatively simple composition, as well as the hygroscopicity of carbonization products ($CaCO_3$ and silica gel), such as γ-C_2S binding material, can be considered as a promising substrate of photocatalysts. In this case, the using of supported TiO_2 in the γ-C_2S carbonated binding material can possibly promote the application efficiency of photocatalysts. The schematic principle of De-NOx by supporting TiO_2 in the γ-C_2S carbonated binding material is shown in Figure 1.

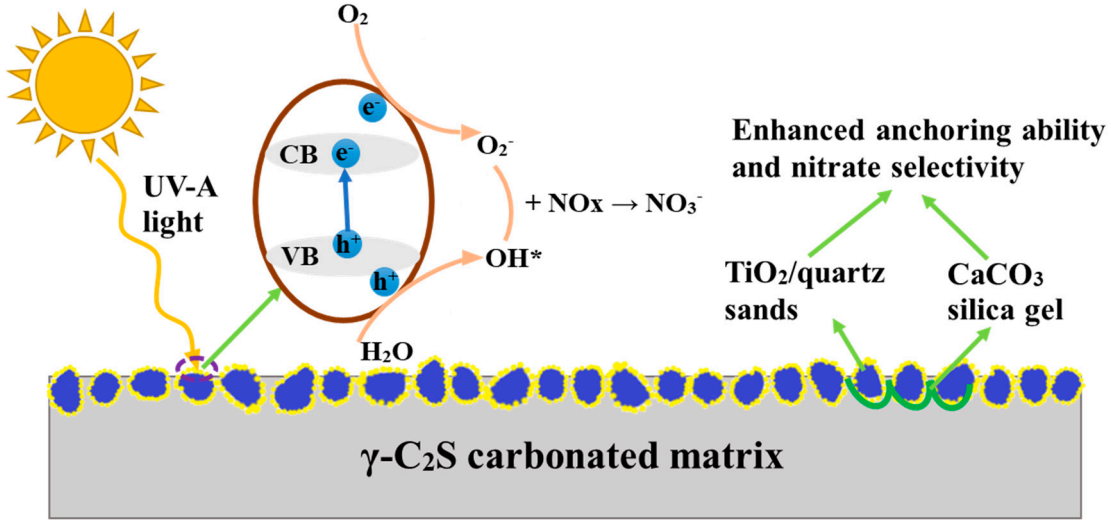

Figure 1. The schematic of De-NOx via photocatalytic oxidation.

Therefore, in this work, we mainly focus on the application technologies and De-NOx and RhB photodegradation performance of supported TiO_2 in γ-C_2S carbonated binding materials (TQSC).

Of which, γ-C_2S was prepared as the substrate material, the quartz sand-supported TiO_2, which is a promising photocatalytic aggregate for application in concrete reported by our previous work [42], was mounted to γ-C_2S carbonated matrix surface with surface mixing methods. The efficiency of De-NOx (degradation of NOx) and its durability were evaluated and compared, respectively. Since rain-washing is an essential factor in its service life, the photocatalytic washing resistance of prepared specimens were also evaluated. We hope the results of this work can shed more light on the preparation of highly cost-efficient photocatalytic building materials.

2. Results and Discussions

2.1. Physical and Chemical Properties

Figure 2 shows the XRD patterns of prepared TiO_2, TiO_2/quartz sand and quartz sand. It can be seen that prepared TiO_2 is an anatase crystal. Compared with the XRD pattern of quartz sand, it can be observed that there is no obvious TiO_2 diffraction peak in TiO_2/quartz sand, which indicates that TiO_2 coating amounts in the particle surface of quartz sand are small or the diffraction peak intensity of quartz is too strong. This is consistent with our previous reports [41]. The coating amounts of TiO_2 on quartz sand surface was therefore tested by XRF, as shown in Table 1; the coating mass fraction of is 0.327%.

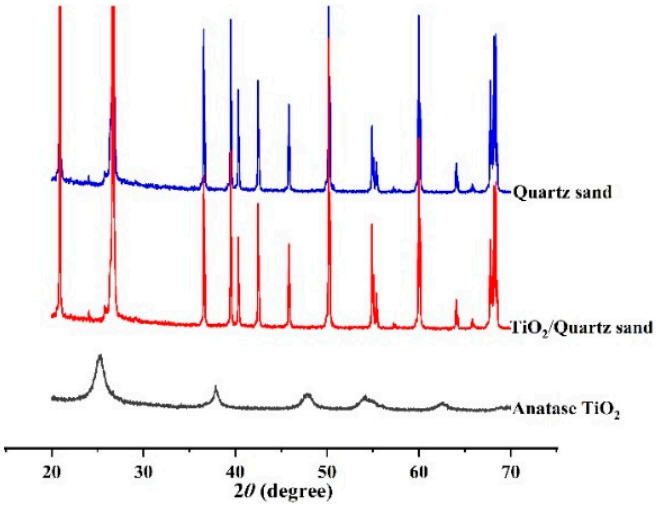

Figure 2. X-ray diffraction (XRD) patterns of quartz sand, TiO_2/quartz sand and pure TiO_2.

Table 1. Chemical compositions of quartz sand and TiO_2/quartz sand.

Chemical Composition (Mass Fraction, %)	Quartz Sand	TiO_2/Quartz Sand
Na_2O	0.037	0.035
Al_2O_3	0.115	0.144
SiO_2	99.695	98.680
P_2O_5	0.036	0.032
SO_3	0.015	0.024
TiO_2	-	0.327

The morphologies of quartz sand and TiO_2/quartz sand can be observed in Figure 3, which show the different surface contrasts. In comparison with uncoated quartz sand (Figure 3(a1,a2)), complete TiO_2 coverage can be directly observed on the surface of TiO_2/quartz sand (Figure 3(b1,b2)). Moreover, the EDS element image (Figure 3(b3,b4)) also indicates that the TiO_2 particles were successfully coated on quartz sand surface, which was similar with our previous reports [43].

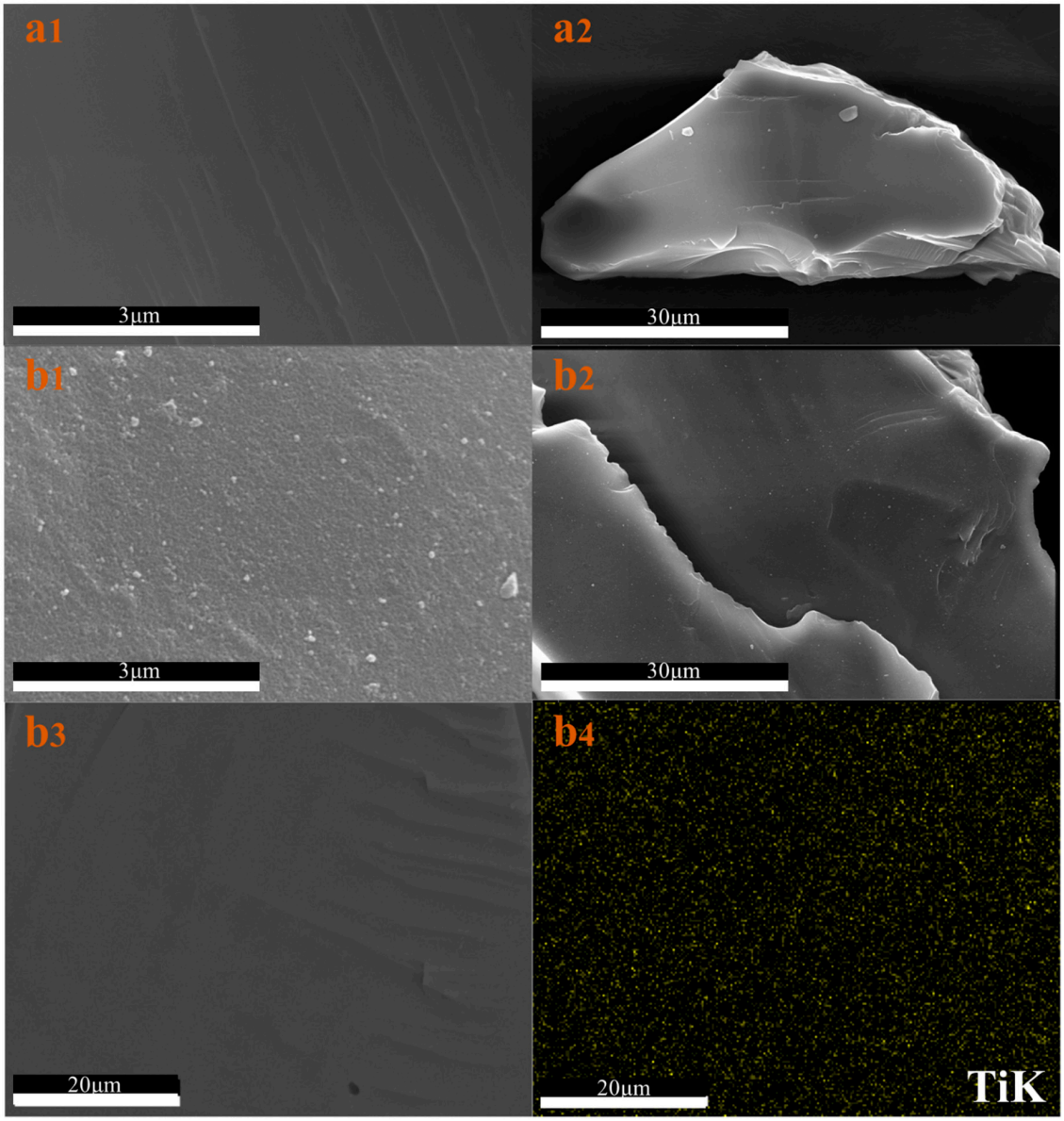

Figure 3. Surface morphologies of pure quartz sand (**a**) and TiO_2/quartz sand (**b**).

Figure 4 shows the surface morphologies of TiO_2/quartz sand in carbonated γ-C_2S matrix with different embedded amounts, and a2, b2, c2, d2 and e2 are the high-resolution images of a1, b1, c1, d1 and e1, respectively. It can be seen that the surface morphologies of TQSC changed and the exposure surface areas of TiO_2/quartz sand gradually increased as increasing embedded amounts. It also can be noticed that the coverage areas of carbonated γ-C_2S on TiO_2/quartz sand seem gradually increases as the embedded amounts of TiO_2/quartz sand decreasing from 100% to 60%, indicating that the supported TiO_2 exposure area is reduced but probably increasing the anchorage force. It is worth to mention that the increase of carbonated products, the amount of micropores on the specimen surface increases, which probably can improve the adsorption ability of gas and increase the nitrate selectivity (S%).

2.2. Photocatalytic Performance

Figure 5 shows the typical NO, NO_2 and NOx concentration curves of prepared quartz sand-supported TiO_2 under light and dark conditions. The photocatalytic procedure of NO can be divided into three stages: firstly, the concentrations of NO and NOx are stable in the dark; secondly,

upon the light illumination, the concentrations of NO and NOx decrease and NO_2 concentration increases until reach a stable level; thirdly, NO and NOx concentrations recover and the concentration of NO_2 returns to initial state after turning off the light.

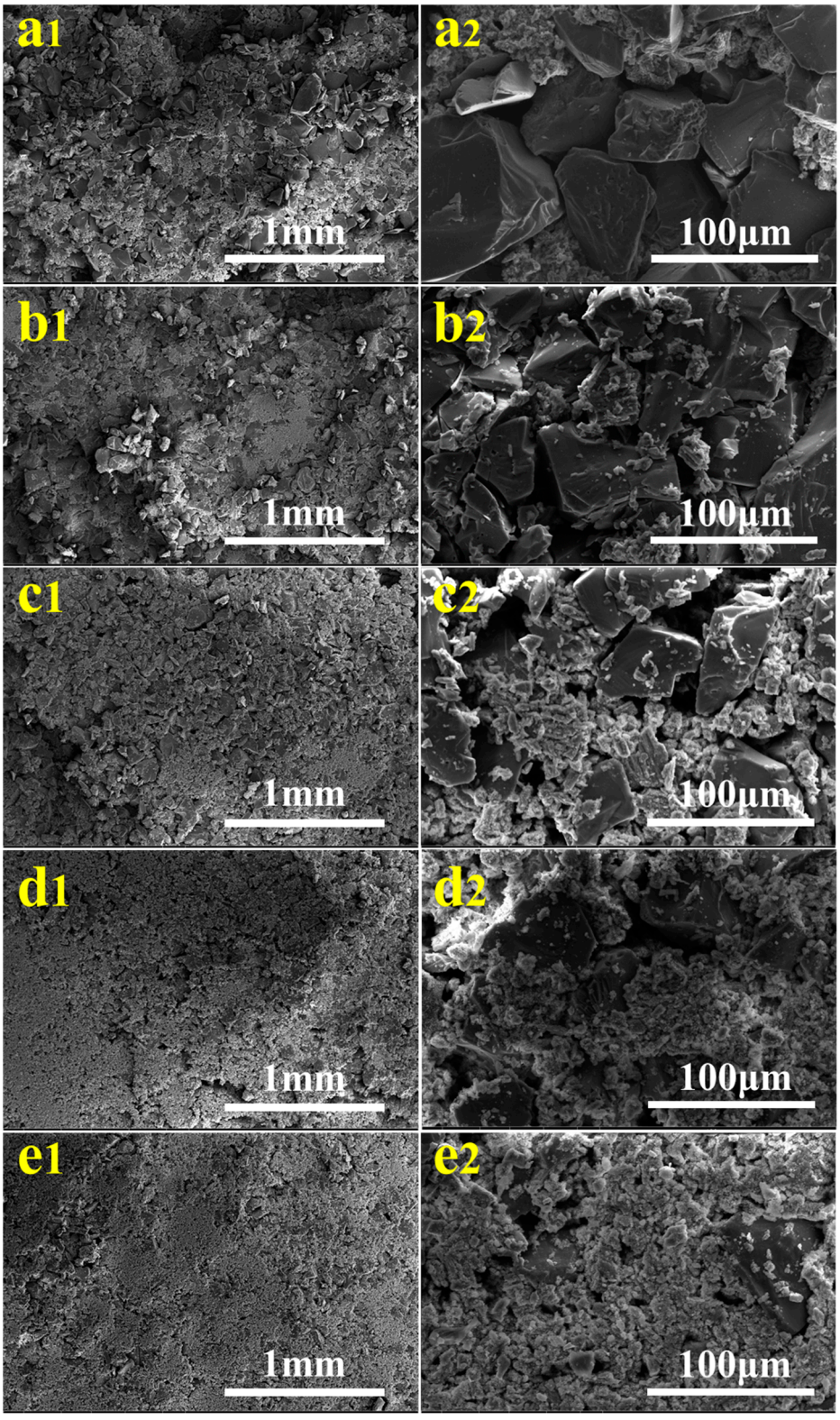

Figure 4. SEM patterns of specimens: (**a**) TQSC-100%; (**b**) TQSC-90%; (**c**) TQSC-80%; (**d**) TQSC-70% and (**e**) TQSC-60%.

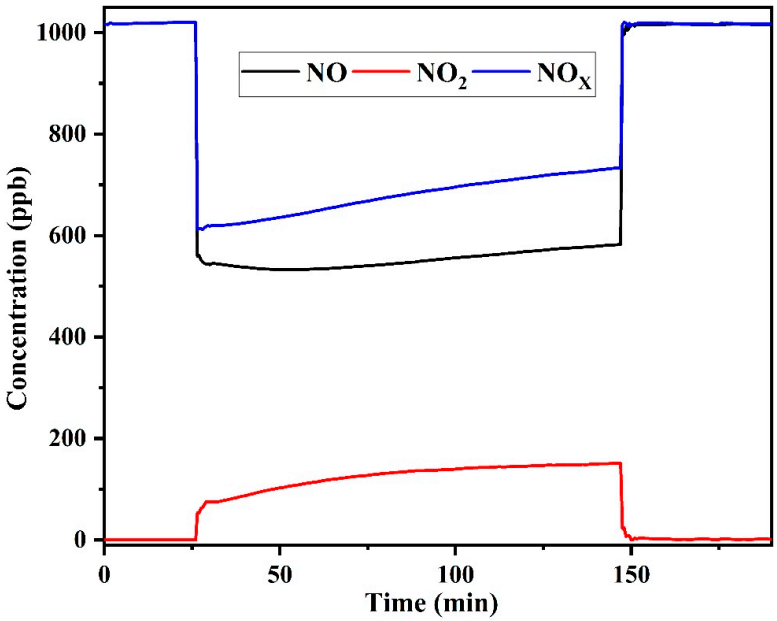

Figure 5. Concentration outlines of NO, NO_2 and NOx for TiO_2/quartz sand during the photocatalytic oxidation of NO.

The photocatalytic performance of TiO_2/quartz sand embedded carbonated $C_2S(\gamma)$ composites (TQSC) are shown in Figure 6. It can be observed that pure γ-C_2S and unloaded quartz sand-$C_2S(\gamma)$ compositions presented almost no efficient on the degradation of NOx, while the photocatalysts supported samples showed the strong NOx degradation ability. It also can be noticed that the photonic efficiency of NO, NOx removal and NO_2 intermediate production decreased obviously with reducing the mass fraction of TiO_2/quartz sand surface mounted amounts, which were contributed to the reduction of TiO_2 exposure surface areas as confirmed by the observation of Figure 4. It should be mentioned that TiO_2/quartz sand mixed specimen showed lower NO, NO_2 and NOx photonic efficiencies than these of TiO_2/quartz sand surface mounted specimens. For NO degradation, the photocatalytic efficiencies of TQSC-100%, TQSC-90%, TQSC-80%, TQSC-70% and TQSC-60% are about 225, 160, 106, 64 and 36 times higher than that of TiO_2/quartz sand mixed sample, respectively. For NOx degradation, the photocatalytic efficiencies are about 142, 103, 69, 46 and 26 times higher, respectively. However, the application amounts of photocatalytic TiO_2 quartz sand in mixed specimen is about 11.7 times higher than that of TQSC-60% specimen. This suggests that TiO_2/quartz sand surface mounted specimens have greater photocatalytic efficiency and better application cost efficient. As shown in Figure 6, for TiO_2/quartz sand surface mounted specimens, the nitrate selectivity (S%) increased slightly with decreasing the mass fraction of TiO_2/quartz sand application amounts, which were associated with the influences of increasing $CaCO_3$ and silica gel. According to our previous work [41], the hygroscopicity of $CaCO_3$ and silica gel can change the humidity of photocatalytic materials, which is beneficial to the improvement of S%. The increase in S% might also be related to the change of surface morphology of the specimens as the observation of Figure 4. With the increase of carbonated products, the amount of micropores on the specimen surface increases, which can improve the adsorption ability of gas and increase the nitrate selectivity (S%).

2.3. Photocatalytic Durability Evaluation

The photocatalytic durability is very important to the real application of photocatalytic concrete regarding to its application efficient and cost efficiency [44,45]. The water-washing test is one of durability evaluation methods to help understand the photocatalytic stability [46,47]. Figure 7 shows the De-NOx photonic efficiencies and nitrate selectivity of TiO_2/quartz sand-supported $C_2S(\gamma)$ carbonated composites before and after the water-washing test. It can be observed that the photonic efficiencies of

NO, NOx removal and NO_2 intermediate production gradually decreased with the increase of washing time. Nevertheless, it should be mentioned that NO, NOx and NO_2 photonic efficiencies decreased fast in the first water-washing cycle, while became stable and stable in the following water-washing cycles. It is worth to mention that the reduction range of NO, NOx and NO_2 photonic efficiencies decrease after the washing time reaches 60 s, and almost stable at 3600 s, which may be associated with the decline of photocatalytic performance of TiO_2/quartz sand or the drop out of photocatalysts from matrix after water-washing [41]. This can likely be attributed to the accumulation of TiO_2/quartz sand on the γ-C_2S carbonated matrix surface, which results in the weak binding performance of some photocatalytic quartz sand and carbonated products. After the initial water-washing, the faster decrease in photonic efficiency for the high-mass fraction of photocatalytic quartz sand (TQSC-100% and TQSC-90%) can provide evidence to the above conclusions.

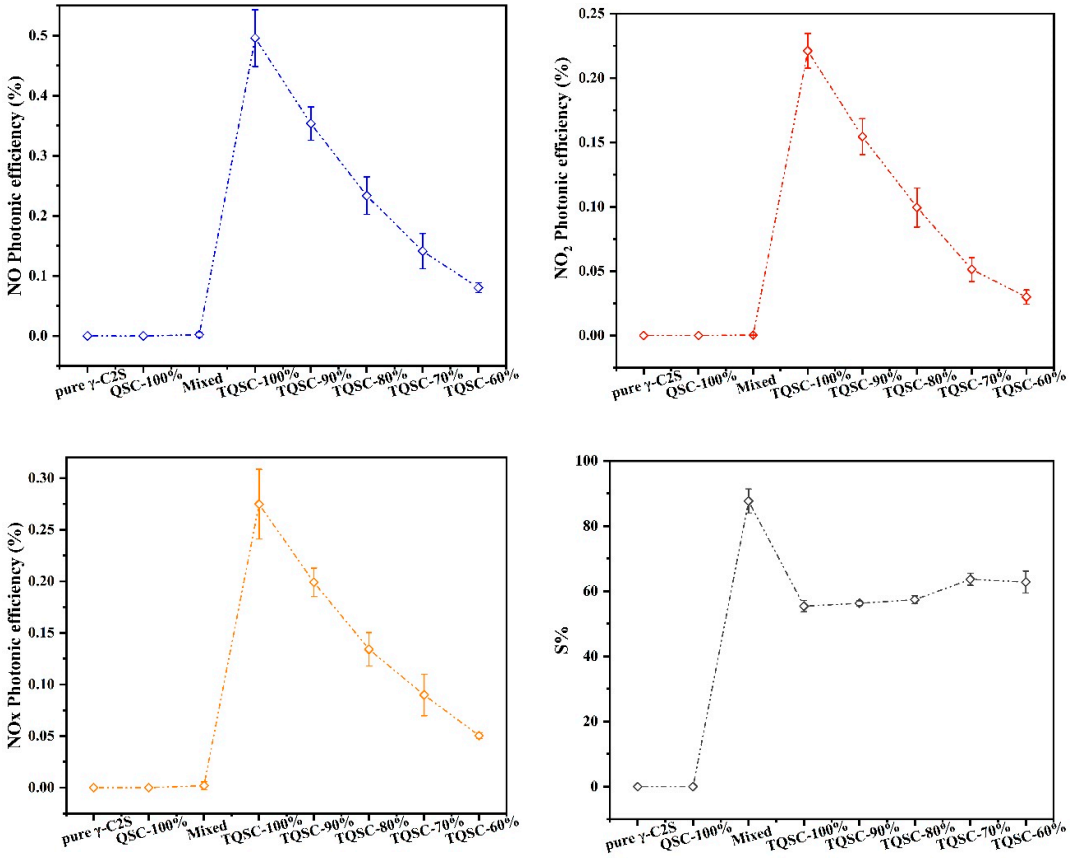

Figure 6. NO, NO_2 and NOx photonic efficiencies and nitrate selectivity (S%) of pure γ-C_2S, QSC-100%, mixed and TQSC specimens.

Figure 7 shows the nitrate selectivity (S%) of each specimen before and after water-washing test. It can be observed that the S% of each sample almost increased with the increase of water-washing time, which probably due to the exposure areas increase of $CaCO_3$ and silica gel, and subsequent increased the adsorbed water of photocatalytic materials surface, which have a positive effect on S% proven by our previous work [41]. It also can be seen that the NO, NOx and NO_2 photonic efficiencies of TiO_2/quartz sand-supported γ-C_2S carbonated composite (TQSC-60%) is relatively stable after a long period of washing, meaning that the photocatalytic durability is better than others.

After water-washing for 3600 s, the self-cleaning performance of TiO_2/quartz sand-supported γ-C_2S carbonated composite (TQSC-60%) was also was studied by the color change of the sample surface under the identical light source of the photocatalytic De-NOx experiment. Figure 8 shows the images taken before and after lamp irradiation 4 h. It can be observed that the RhB (rhodamine B, 20 mg·L^{-1}, 1 mL) coated pure γ-C_2S surface has almost no color change after light irradiation, but the

color in washed-TQSC-60% surface almost faded, which indicates that the TiO_2/quartz sand-supported $C_2S(\gamma)$ carbonated composites still maintained its photocatalytic performance under light irradiation after a long period of water-washing, and the washed-TQSC-60% also present the excellent self-cleaning ability to photocatalytic degradation of rhodamine B.

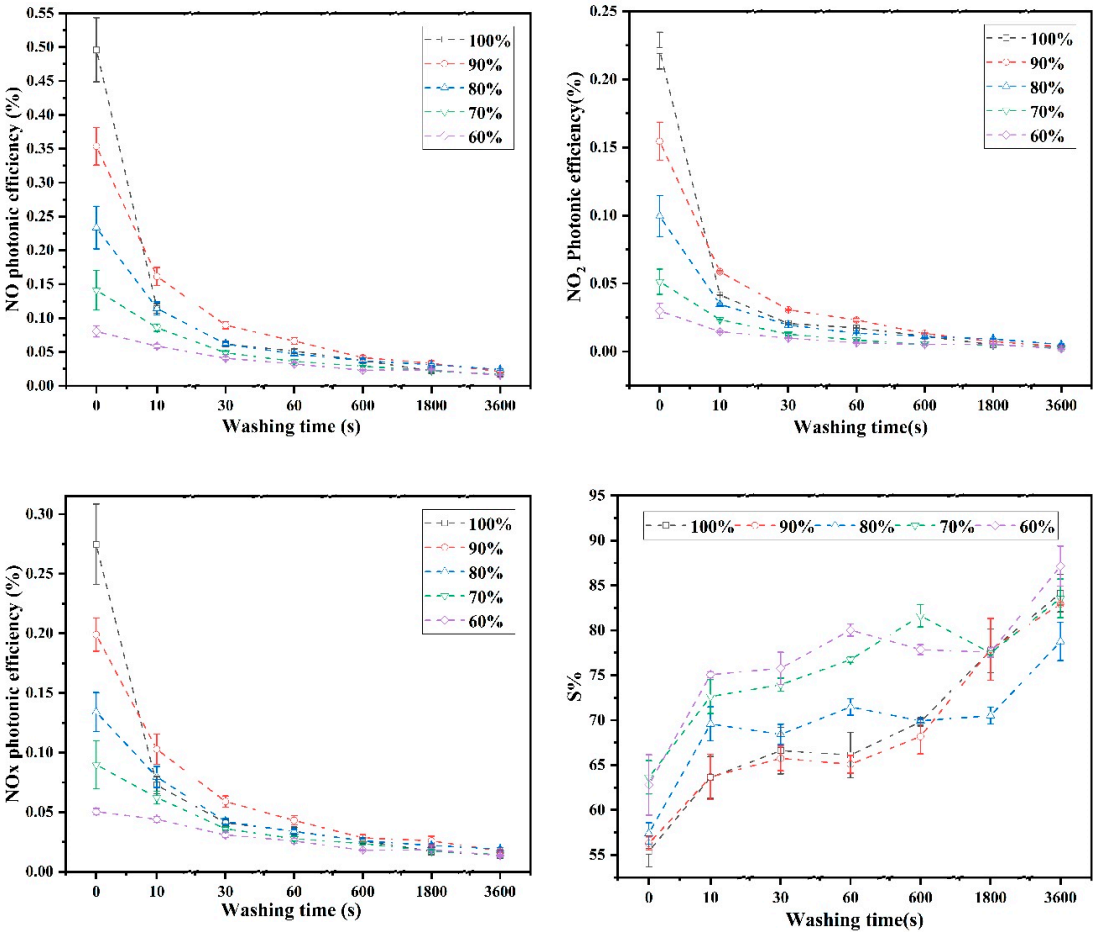

Figure 7. De-NOx photonic efficiencies and nitrate selectivity (S%) of quartz sand-supported TiO_2-$C_2S(\gamma)$ compositions before and after the washing test.

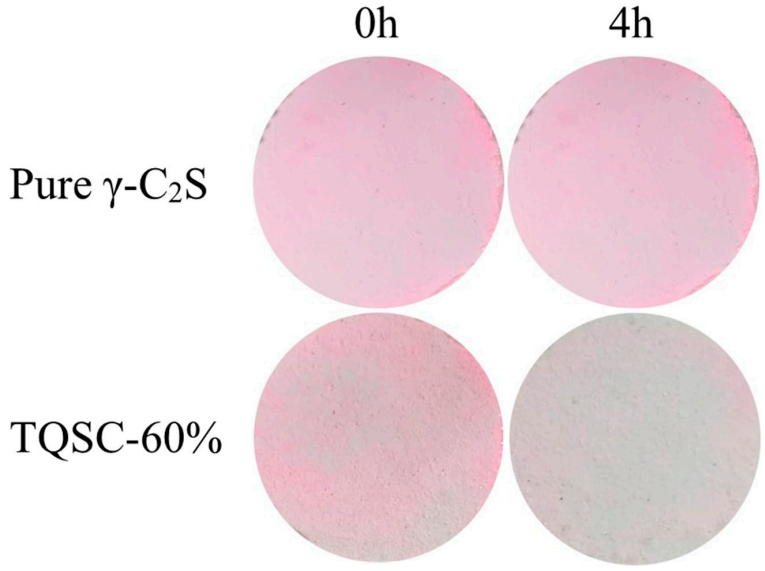

Figure 8. Color variation of RhB coated on pure γ-C_2S and washed-TQSC-60%.

3. Materials and Methods

3.1. Materials

The γ-C_2S used in this study was produced by $Ca(OH)_2$ and SiO_2, which was calcined at 1400 °C for 3 h, and then cooled in the natural atmosphere [48]. The quartz sand with 0.075–0.107 mm diameter was used to support TiO_2 photocatalysts in this study. Sodium hydroxide (NaOH, 0.1 M), C_2H_5OH (absolute ethanol, 99.9%), titanium tetra-isopropoxide (TTIP, 99.9%) and CH_3COOH (acetic acid, 99.6%) were purchased from Sinopharm Chemical Reagent Co. Ltd. Deionized water was used throughout the process of sample preparation.

3.2. Methods

3.2.1. TiO_2 Hydrosol Preparation

TiO_2 hydrosol was synthesized based on a low temperature precipitation–peptization method [41,49]. The preparation method are as follows. Ten mL of titanium tetra-isopropoxide and 30 mL of absolute ethanol were mixed with stirring for 30 min at room temperature. Then, the mixed solution was dropwise added into the other mixture (reaction solution pH = 2.29), which contained 8 mL of CH_3COOH and 160 mL of deionized water. After that, the obtained suspension was stirred for 48 h at 50 °C, and then aged for 72 h at room temperature. The specific surface area of obtained TiO_2 catalysts was 177.85 $m^2 \cdot g^{-1}$.

3.2.2. TiO_2 Supported Quartz Sands Preparation

The method of preparing TiO_2-coated quartz sand (TQS) is as follows. Before coating TiO_2 on quartz sand with 0.075–0.107 mm diameter, the sand was treated with 0.1 M NaOH for 24 h to maximize the hydroxide groups of the surface. Subsequently, the alkaline treated quartz sand was washed with deionized water three times and dried at 105 °C for 24 h. After that, the obtained quartz sand was distributed uniformly immersed in the prepared TiO_2 hydrosol suspension for 5 min. The resulting mixture was filtrated and then dried at 105 °C for 24 h to produce TQS. The specific surface area of TiO_2/quartz sand was 42.83 $m^2 \cdot g^{-1}$.

3.2.3. Photocatalytic γ-C_2S Carbonated Matrix Preparation

The preparation route of photocatalytic γ-C_2S carbonated matrix is shown in Figure 9, it can be divided to compaction and carbonization steps. For TiO_2/quartz sand surface-mounted samples, the detail preparation steps are as follows: 1.5 g of prepared TiO_2/quartz sand (TQS) and a certain amount of γ-C_2S slurry (water/γ-C_2S mass ratio = 0.15 [48]) were mixed uniformly, and then the mixture was uniformly distributed on the bottom of steel mould (100 mm length × 100 mm width × 50 mm height), after that, 35 g of γ-C_2S and 5.25 g of water were mixed for 2 min followed by spreading on the top layer. Subsequently, the steel mould was compacted until the displayed pressure reached 40 MPa for 1 min. In order to expediently de-mould, the specimen was pre-carbonated in the bucket for 1 h before unmolding. The pre-carbonated specimen was then put into the carbonation tank curing for 3 h at 0.3 MPa pressure. Finally, TQS-surface-mounted γ-C_2S carbonated matrix was prepared, which marked as TQSC specimen. For comparison, TQS surface mounted mass fractions were set as 100%, 90%, 80%, 70% and 60% to total mass of surface TQS/γ-C_2S, respectively. The prepared specimens were denoted as TQSC-m, where m was the mass fraction of TQS on the surface (m = 100%, 90%, 80%, 70% and 60%).

In addition, pure quartz sand surface-mounted and pure γ-C_2S samples via foregoing method also were prepared for comparison, which were denoted as QSC-100% and pure γ-C_2S, respectively. TQS dispersed in γ-C_2S matrix sample was also prepared, the mixing amounts of TQS was 10.5 g. The obtained TiO_2/quartz sand blended γ-C_2S matrix specimen was denoted as mixed.

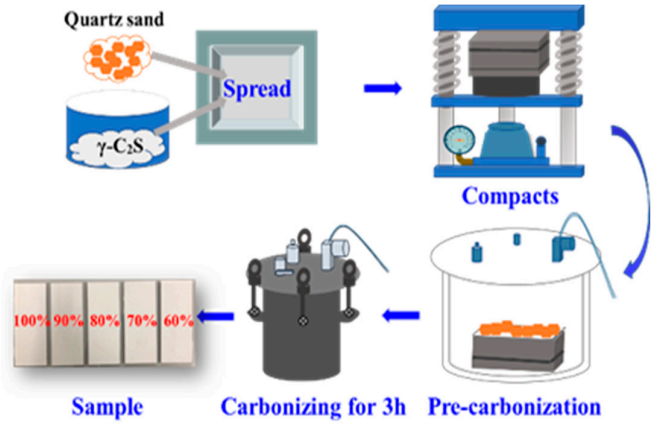

Figure 9. Preparation schematic diagram of photocatalytic γ-C_2S carbonated matrix.

3.3. Characterization

The X-ray diffraction (XRD) pattern was conducted by a D8 Advance X-ray diffractometer (BRUKER AXS GMBH, Karlsruhe, Germany) with Cu Kα radiation, the test 2θ value ranging was 20–70° with 6°·min^{-1} scanning speed. The loading quantity of TiO_2 on quartz sand was obtained by quantitative X-ray fluorescence (XRF, Zetium). Surface morphology and elemental composition of specimens were observed by scanning electron microscope (SEM, FEI QUANTA FEG 450, FEI Company, Hillsboro, OR, USA) equipped with energy-dispersive X-ray spectroscopy (EDS) analysis at ca.10 mm working distance and accelerating voltage of 15 and 20 kV.

3.4. Photocatalytic Performance

3.4.1. Photocatalytic Removal of NOx

The photocatalytic efficiencies of the prepared photocatalytic specimens were evaluated by the degradation ability of NOx in the ISO reactor, schematically illustrated in Figure 10. The sample was placed inside the ISO reactor and irradiated by a 300 W Xe-lamp solar simulator (CEL-HXF300, CeauLight Co., Ltd., Beijing, China), adjusting the distance between the reactor and lamp to acquire that the photon flux on the surface of sample was measured to be 3.05×10^{-6} mol·s^{-1}·m^{-2}. 1 ppm of NO in synthesized air, conditioned at a 50% relative humidity and 25 °C of the test environment temperature, was passed through the reactor with a flow velocity of 5×10^{-5} m^3·s^{-1}. The concentrations of NO, NO_2 and NOx were continuously measured by a NO-NO_2-NOx analyzer (HN-CK5001, Taiyuan Hainachenke Instrument Co., Ltd., Taiyuan China). Each specimen was measured in the dark until the equilibrium concentration of NO, NO_2 and NOx was reached. And then, under the illumination until NO, NO_2 and NOx concentrations reached steady state. After that, each sample was measured in the dark again until steady state concentrations were observed. For comparison, the photocatalytic performance of carbonated pure γ-C_2S plate, TiO_2 supported/unsupported quartz sand composite and photocatalytic quartz sand dispersed in γ-C_2S substrate specimens were measured under the identical conditions and testing procedure. The photonic efficiency (ξ) of NOx, NO and NO_2 was calculated according to Equation (1). The catalyst selectivity for nitrate (S%) was calculated according to Equation (2) [50].

$$\xi = \frac{(C_d - C_i)VP}{\Phi ART} \times 100\% \quad (1)$$

$$S\% = \frac{\xi_{NOx}}{\xi_{NO}} \times 100 \quad (2)$$

where C_d is the concentration of NOx, NO or NO_2 in the dark; C_i is the concentration of NOx, NO or NO_2 under the light irrigation; V (m^3·s^{-1}) is the volumetric flow rate; P (Pa) is the pressure; Φ (mol·s^{-1}·m^2) is the photon flux impinging the surface; A (m^2) is the irradiated specimen area; R (J·mol^{-1}·K^{-1}) is the gas constant; T (K) is the temperature.

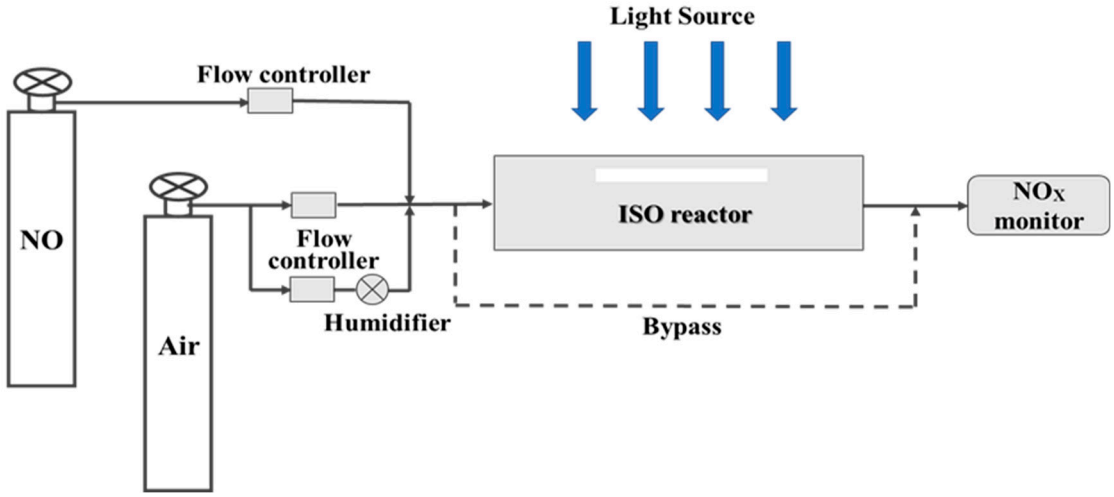

Figure 10. Schematic diagram of photocatalytic reaction for NOx degradation.

3.4.2. Photocatalytic Degradation of RhB

The photocatalytic degradation of RhB was evaluated according to the previously reported literature [51–54]. Typically, the prepared plastic with a diameter of 20 mm was glued to the surface of as-prepared sample. 1 mL rhodamine B solution at a concentration of 20 mg·L^{-1} was uniformly spread to the specimen surface within the plastic ring. And then, the specimens were dried at 40 °C for 12 h to solvent drying and dye adsorption. After that, a dried sample was placed under a 300 W xenon lamp (CEL-HXF300, CeauLight Co., Ltd. China), and the distance between the sample and the lamp was adjusted to obtain the illumination intensity of 1 mW·cm^{-2} on the sample surface. The RhB photodegradation was performed by measuring the color change on the sample surface when the irradiation time was 4 h.

3.5. Evaluation of Photocatalytic Durability

To study photocatalytic durability of prepared samples, a rain wash simulator was employed. The schematic diagram and test device of washing resistance were shown in Figure 11. The specific testing procedure is as follows: the surface of resulting specimens was washed with 450 mL·min^{-1} of deionized water at room temperature for 10 s and dried at 105 °C for 12 h. And then, the dried samples were carried out the photocatalytic measurement. The total process was repeated five times, and the other washing times were 30 s, 60 s, 600 s, 1800 s, 3600 s, respectively.

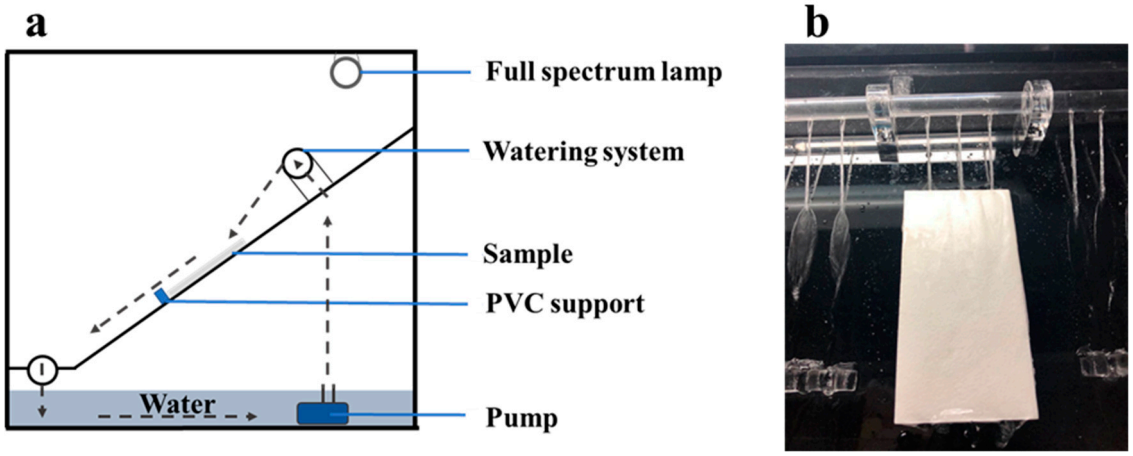

Figure 11. Washing test: (**a**) Schematic diagram; (**b**) top view of the washing test.

4. Conclusions

Based on the environmental friendliness and rapid carbonization/hardening of γ-C_2S carbonated binding materials, the TiO_2/quartz sand-supported $C_2S(\gamma)$ carbonated composites (TQSC) and photocatalytic quartz sand was prepared. In doing so, their physicochemical properties, photocatalytic performance and durability to NOx and RhB were investigated in detail. The characterization results of XRD, SEM and XRF confirmed a uniform TiO_2 layer in quartz sand surface was formed, and the TiO_2/quartz sand mass fraction (MF) is 0.327%. The experimental results showed that with a decrease in the mounted amounts of TiO_2/quartz sand in γ-C_2S carbonated matrix surface, more photocatalytic quartz sand would be covered by γ-C_2S carbonated products, resulting in the reduction of De-NOx performance. All TQSC specimens showed higher De-NOx efficiency than that of the mixed specimen, confirming greater photocatalytic efficiency and low-price advantages of TiO_2/quartz sand-$C_2S(\gamma)$ carbonated composites. After water-washing, the De-NOx efficiencies of TQSC specimens decreased fast in the initial time but would become stable after 3600 s of water-washing. In compared with the pure sample, the relatively high performance of De-NOx and the good self-cleaning effect of RhB on the water-washed TQSC-60% specimen can be considered to be a promising photocatalytic product for real applications.

Author Contributions: Conceptualization H.S., L.Y.; methodology H.S., L.Y.; software, H.S.; investigation H.S., Y.F.; writing—original draft preparation H.S., L.Y.; supervision L.Y. All authors have read and agreed to the published version of the manuscript.

Funding: This research was funded by the Natural Science Foundation of China (No. 51802238 and 51925205) and the Fundamental Research Funds for the Central Universities (WUT2018IVA011, WUT2018III022, 2019IVB060, 2020-zy-015, 2020-zy-016).

Conflicts of Interest: The authors declare no conflict of interest.

References

1. Asim, N.; Alghoul, M.; Mohammad, M.; Amin, M.H.; Akhtaruzzaman, M.; Amin, N.; Sopian, K. Emerging sustainable solutions for depollution: Geopolymers. *Constr. Build. Mater.* **2019**, *199*, 540–548. [CrossRef]
2. Pérez-Nicolás, M.; Balbuena, J.; Cruz-Yusta, M.; Sánchez, L.; Navarro-Blasco, I.; Fernández, J.M.; Alvarez, J.I. Photocatalytic NOx abatement by calcium aluminate cements modified with TiO_2: Improved NO_2 conversion. *Cem. Concr. Res.* **2015**, *70*, 67–76. [CrossRef]
3. Jin, Q.; Saad, E.M.; Zhang, W.; Tang, Y.; Kurtis, K.E. Quantification of NOx uptake in plain and TiO_2-doped cementitious materials. *Cem. Concr. Res.* **2019**, *122*, 251–256. [CrossRef]
4. Guo, M.Z.; Chen, J.; Xia, M.; Wang, T.; Poon, C.S. Pathways of conversion of nitrogen oxides by nano TiO_2 incorporated in cement-based materials. *Build. Environ.* **2018**, *144*, 412–418. [CrossRef]
5. Melo, J.V.S.D.; Trichês, G. Evaluation of the influence of environmental conditions on the efficiency of photocatalytic coatings in the degradation of nitrogen oxides (NOx). *Build. Environ.* **2012**, *49*, 117–123. [CrossRef]
6. Qian, C.X.; Zhao, L.F.; Fu, D.F.; Li, L.; Wang, R.X. Study on the effect of temperature, humidity and light intensity on photocatalytic oxidation of NO_2 by Nano-TiO_2 immobilized on cement-based materials. *J. Environ. Sci. China* **2005**, *25*, 623–630. [CrossRef]
7. Mills, A.; Elouali, S. The nitric oxide ISO photocatalytic reactor system: Measurement of NOx removal activity and capacity. *J. Photochem. Photobiol. A Chem.* **2015**, *305*, 29–36. [CrossRef]
8. Gauvin, F.; Caprai, V.; Yu, Q.L.; Brouwers, H.J.H. Effect of the morphology and pore structure of porous building materials on photocatalytic oxidation of air pollutants. *Appl. Catal. B Environ.* **2018**, *227*, 123–131. [CrossRef]
9. Strini, A.; Cassese, S.; Schiavi, L. Measurement of benzene, toluene, ethylbenzene and o-xylene gas phase photodegradation by titanium dioxide dispersed in cementitious materials using a mixed flow reactor. *Appl. Catal. B Environ.* **2005**, *61*, 90–97. [CrossRef]
10. Mills, A.; Hill, C.; Robertson, P.K.J. Overview of the current ISO tests for photocatalytic materials. *J. Photochem. Photobiol. A Chem.* **2012**, *237*, 7–23. [CrossRef]

11. Hakki, A.; Yang, L.; Wang, F.; Macphee, D.E. The Effect of Interfacial Chemical Bonding in TiO_2-SiO_2 Composites on Their Photocatalytic NOx Abatement Performance. *J. Vis. Exp.* **2017**, *125*, e56070. [CrossRef]
12. Fujishima, M.; Takatori, H.; Tada, H. Interfacial chemical bonding effect on the photocatalytic activity of TiO_2-SiO_2 nanocoupling systems. *J. Colloid Interface Sci.* **2011**, *361*, 628–631. [CrossRef]
13. Maggos, T.; Bartzis, J.G.; Liakou, M.; Gobin, C. Photocatalytic degradation of NOx gases using TiO_2-containing paint: A real scale study. *J. Hazard. Mater.* **2007**, *146*, 668–673. [CrossRef] [PubMed]
14. Guo, M.Z.; Poon, C.S. Photocatalytic NO removal of concrete surface layers intermixed with TiO_2. *Build. Environ.* **2013**, *70*, 102–109. [CrossRef]
15. Jimenez-Relinque, E.; Rodriguez-Garcia, J.R.; Castillo, A.; Castellote, M. Characteristics and efficiency of photocatalytic cementitious materials: Type of binder, roughness and microstructure. *Cem. Concr. Res.* **2015**, *71*, 124–131. [CrossRef]
16. Chen, J.; Poon, C.S. Photocatalytic cementitious materials: Influence of the microstructure of cement paste on photocatalytic pollution degradation. *Environ. Sci. Technol.* **2009**, *43*, 8948–8952. [CrossRef]
17. Lucas, S.; Ferreira, V.; De Aguiar, J.B. Incorporation of titanium dioxide nanoparticles in mortars—Influence of microstructure in the hardened state properties and photocatalytic activity. *Cem. Concr. Res.* **2013**, *43*, 112–120. [CrossRef]
18. Cassar, L. Photocatalysis of Cementitious Materials: Clean Buildings and Clean Air. *Mrs Bull.* **2004**, *29*, 328–331. [CrossRef]
19. Ballari, M.M.; Yu, Q.L.; Brouwers, H.J.H. Experimental study of the NO and NO_2 degradation by photocatalytically active concrete. *Catal. Today* **2011**, *161*, 175–180. [CrossRef]
20. Martinez, T.; Bertron, A.; Ringot, E.; Escadeillas, G. Degradation of NO using photocatalytic coatings applied to different substrates. *Build. Environ.* **2011**, *46*, 1808–1816. [CrossRef]
21. Faraldos, M.; Kropp, R.; Anderson, M.A.; Sobolev, K. Photocatalytic hydrophobic concrete coatings to combat air pollution. *Catal. Today* **2015**, *259*, 228–236. [CrossRef]
22. Guo, M.Z.; Ling, T.C.; Poon, C.S. Photocatalytic NOx degradation of concrete surface layers intermixed and spray-coated with nano-TiO_2: Influence of experimental factors. *Cem. Concr. Compos.* **2017**, *83*, 279–289. [CrossRef]
23. Boonen, E.; Beeldens, A. Photocatalytic roads: From lab tests to real scale applications. *Eur. Transp. Res. Rev.* **2013**, *5*, 79–89. [CrossRef]
24. Macphee, D.E.; Folli, A. Photocatalytic concretes—The interface between photocatalysis and cement chemistry. *Cem. Concr. Res.* **2016**, *85*, 48–54. [CrossRef]
25. Guo, M.Z.; Maury-Ramirez, A.; Poon, C.S. Self-cleaning ability of titanium dioxide clear paint coated architectural mortar and its potential in field application. *J. Clean. Prod.* **2016**, *112*, 3583–3588. [CrossRef]
26. Bocci, E.; Riderelli, L.; Fava, G.; Bocci, M. Durability of NO oxidation effectiveness of pavement surfaces treated with photocatalytic Titanium Dioxide. *Arabian J. Sci. Eng.* **2016**, *41*, 4827–4833. [CrossRef]
27. Bianchi, C.L.; Pirola, C.; Galli, F.; Cerrato, G.; Morandi, S.; Capucci, V. Pigmentary TiO_2: A challenge for its use as photocatalyst in NOx air purification. *Chem. Eng. J.* **2015**, *261*, 76–82. [CrossRef]
28. Todorova, N.; Giannakopoulou, T.; Karapati, S.; Petridis, D.; Vaimakis, T.; Trapalis, C. Composite TiO_2/clays materials for photocatalytic NOx oxidation. *Appl. Surf. Sci.* **2014**, *319*, 113–120. [CrossRef]
29. Kamaruddin, S.; Stephan, D. Quartz–titania composites for the photocatalytical modification of construction materials. *Cem. Concr. Compos.* **2013**, *36*, 109–115. [CrossRef]
30. Folli, A.; Pochard, I.; Nonat, A.; Jakobsen, U.H.; Shepherd, A.M.; Macphee, D.E. Engineering Photocatalytic Cements: Understanding TiO_2 Surface Chemistry to Control and Modulate Photocatalytic Performances. *J. Am. Ceram. Soc.* **2010**, *93*, 3360–3369. [CrossRef]
31. Folli, A.; Pade, C.; Hansen, T.B.; Marco, T.D.; Macphee, D.E. TiO_2 photocatalysis in cementitious systems: Insights into self-cleaning and depollution chemistry. *Cem. Concr. Res.* **2012**, *42*, 539–548. [CrossRef]
32. Karatasios, I.; Katsiotis, M.S.; Likodimos, V.; Kontos, A.I.; Papavassiliou, G.; Falaras, P.; Kilikoglou, V. Photo-induced carbonation of lime-TiO_2 mortars. *Appl. Catal. B Environ.* **2010**, *95*, 78–86. [CrossRef]
33. Tsang, C.H.A.; Li, K.; Zeng, Y.; Zhao, W.; Zhang, T.; Zhan, Y.; Xie, R.; Leung, D.Y.C.; Huang, H. Titanium oxide based photocatalytic materials development and their role of in the air pollutants degradation: Overview and forecast. *Environ. Int.* **2019**, *125*, 200–228. [CrossRef]
34. Yang, L.; Wang, F.; Shu, C.; Liu, P.; Zhang, W.; Hu, S.; Yang, L.; Wang, F.; Shu, C.; Liu, P. TiO_2/porous cementitious composites: Influences of porosities and TiO_2 loading levels on photocatalytic degradation of gaseous benzene. *Constr. Build. Mater.* **2017**, *150*, 774–780. [CrossRef]

35. Sugrañez, R.; Álvarez, J.; Cruz-Yusta, M.; Mármol, I.; Morales, J.; Vila, J.; Sánchez, L. Enhanced photocatalytic degradation of NOx gases by regulating the microstructure of mortar cement modified with titanium dioxide. *Build. Environ.* **2013**, *69*, 55–63. [CrossRef]
36. Karapati, S.; Giannakopoulou, T.; Todorova, N.; Boukos, N.; Dimotikali, D.; Trapalis, C. Eco-efficient TiO_2 modification for air pollutants oxidation. *Appl. Catal. B Environ.* **2015**, *176–177*, 578–585. [CrossRef]
37. Mu, Y.; Liu, Z.; Wang, F.; Huang, X. Effect of barium doping on carbonation behavior of γ-C_2S. *J. CO_2 Util.* **2018**, *27*, 405–413. [CrossRef]
38. Guan, X.M.; Liu, S.H.; Feng, C.H.; Qiu, M. The hardening behavior of γ-C_2S binder using accelerated carbonation. *Constr. Build. Mater.* **2016**, *114*, 204–207. [CrossRef]
39. Chang, J.; Fang, Y.; Shang, X. The role of β-C_2S and γ-C_2S in carbon capture and strength development. *Mater. Struct.* **2016**, *49*, 4417–4424. [CrossRef]
40. Shi, C.J.; Bo, Q.; John, L.P. Recent progress in low-carbon binders. *Cem. Concr. Res.* **2019**, *122*, 227–250. [CrossRef]
41. Yang, L.; Hakki, A.; Wang, F.; Macphee, D.E. Photocatalyst efficiencies in concrete technology: The effect of photocatalyst placement. *Appl. Catal. B Environ.* **2018**, *222*, 200–208. [CrossRef]
42. Zheng, L.; Jones, M.R.; Yang, L.; Hakki, A.; Macphee, D.E. Exposed-aggregate areas and photocatalytic efficiency of photocatalytic aggregate mortar. *Mag. Concr. Res.* **2020**, *72*, 852–863. [CrossRef]
43. Yang, L.; Hakki, A.; Zheng, L.; Jones, M.R.; Wang, F.; Macphee, D.E. Photocatalytic concrete for NOx abatement: Supported TiO_2 efficiencies and impacts. *Cem. Concr. Res.* **2019**, *116*, 57–64. [CrossRef]
44. Boonen, E.; Beeldens, A.; Dirkx, I.; Bams, V. Durability of Cementitious Photocatalytic Building Materials. *Catal Today* **2017**, *287*, 196–202. [CrossRef]
45. Enea, D.; Bellardita, M.; Scalisi, P.; Alaimo, G.; Palmisano, L. Effects of weathering on the performance of self-cleaning photocatalytic paints. *Cem. Concr. Compos.* **2019**, *96*, 77–86. [CrossRef]
46. Yang, Y.; Ji, T.; Su, W.; Kang, Y.; Wu, Y.; Zhang, Y. Enhanced washing resistance of photocatalytic exposed aggregate cementitious materials based on g-C_3N_4 nanosheets-recycled asphalt pavement aggregate composites. *Constr. Build. Mater.* **2019**, *228*, 116748. [CrossRef]
47. Veltri, S.; Palermo, A.M.; De Filpo, G.; Xu, F. Subsurface treatment of TiO_2 nanoparticles for limestone: Prolonged surface photocatalytic biocidal activities. *Build. Environ.* **2019**, *149*, 655–661. [CrossRef]
48. Mu, Y.; Liu, Z.; Wang, F. Comparative Study on the Carbonation-Activated Calcium Silicates as Sustainable Binders: Reactivity, Mechanical Performance, and Microstructure. *ACS Sustain. Chem. Eng.* **2019**, *7*, 7058–7070. [CrossRef]
49. Burunkaya, E.; Akarsu, M.; Erdem Çamurlu, H.; Kesmez, Ö.; Yeşil, Z.; Asiltürk, M.; Arpaç, E. Production of stable hydrosols of crystalline TiO_2 nanoparticles synthesized at relatively low temperatures in diverse media. *Appl. Surf. Sci.* **2013**, *265*, 317–323. [CrossRef]
50. Yang, L.; Hakki, A.; Wang, F.; Macphee, D.E. Different Roles of Water in Photocatalytic DeNOx Mechanisms on TiO_2: Basis for Engineering Nitrate Selectivity? *ACS Appl. Mater. Interfaces* **2017**, *9*, 17034–17041. [CrossRef]
51. Yang, Y.; Ji, T.; Su, W.; Yang, B.; Zhang, Y.; Yang, Z. Photocatalytic NOx abatement and self-cleaning performance of cementitious composites with g-C_3N_4 nanosheets under visible light. *Constr. Build. Mater.* **2019**, *225*, 120–131. [CrossRef]
52. Kim, J.H.; Kim, H.G.; Qudoos, A.; Ryou, J.S. Effect of leaching on the hardened, microstructural and self-cleaning characteristics of titanium dioxide containing cement mortars. *Constr. Build. Mater.* **2019**, *207*, 640–650. [CrossRef]
53. Chen, J.; Kou, S.C.; Poon, C.S. Photocatalytic cement-based materials: Comparison of nitrogen oxides and toluene removal potentials and evaluation of self-cleaning performance. *Build. Environ.* **2011**, *46*, 1827–1833. [CrossRef]
54. Shen, W.G.; Zhang, C.; Li, Q.; Zhang, W.S.; Cao, L.; Ye, J.Y. Preparation of titanium dioxide nano particle modified photocatalytic self-cleaning concrete. *J. Clean. Prod.* **2015**, *87*, 762–765. [CrossRef]